

Supporting Information

Graphene-bridged Multifunctional Flexible Fiber

Supercapacitor with High Energy Density

Libo Gao ^{1,2} Ψ , Jian Song ³ Ψ , James Utama Surjadi ¹, Ke Cao ¹, Ying Han ¹, Dong Sun ¹,

Xiaoming Tao ³ and Yang Lu ^{1,2*}

¹ Department of Mechanical Engineering, City University of Hong Kong, Hong Kong SAR, Kowloon 999077, Hong Kong;

² Shenzhen Research Institute, City University of Hong Kong, Shenzhen 518057, China;

³ Nanotechnology Center of Functional and Intelligent Textiles and Apparel Institute of Textiles and Clothing, The Hong Kong Polytechnic University, 999077, Hong Kong;

Ψ These authors contributed equally to this work.

* E-Mail: yanglu@cityu.edu.hk ;

Materials and methods

Fabrication of the CF-NF (copper foam-nickel fiber)

The CF-NF was synthesized through hydrogen template method. Briefly, the wasted NF was pretreated with acetone, ethanol, HCl solution respectively for 15 min. Then the NF was directly regarded as the negative electrode to deposit the CF in a solution of 0.04 M CuSO₄, 0.5 M H₂SO₄, and 50 mM HCl solution. While the Pt foil (1×1 cm²) was served as the positive electrode. Then the NF with 400 μm was carefully pulled from the solution after electrodeposited for 1 min at a current density of 1 A cm⁻². After gently washed with DI water sufficiently, the CF-NF fiber was put naturally dried at room temperature (RT). The diameter of the fiber was estimated to be 500 μm.

Fabrication of the GSs (Graphene sheets) @CF-NF

For the Fabrication of GSs@CF-NF, simple “dip-coating” method was employed. Before coating, oxygen plasma was employed to make it hydrophilic. Highly concentrated graphene ink solution (2 mg mL⁻¹) was purchased from CARBON VALLEY company. Briefly, the CF-NF was immersed vertically into the prepared solution for 1 min and then slowly pulled from the solution with following drying process using hot-air blower. This simple procedure was repeated for 5 times to certify the homogeneous and sufficient coating.

Fabrication of the NiCo LDH@GSs@CF-NF

Similarly, the GSs@CF-NF was treated with oxygen for 1 min also prior to deposition of the NiCo LDH. The electrodeposition procedure was same with our previous report.^{1,2} Here, in this experiment, the treated fiber was directly electrodeposited the battery-type electrode materials through three-electrode route, in which 4 mM Co(NO₃)₂•6H₂O and 4 mM Ni(NO₃)•6H₂O were regarded as the electrolyte, while Pt electrode was the counter electrode and a saturated calomel electrode (SCE) was the reference electrode. After electrodeposited at -1 V for 12 min, the sample was carefully washed with DI water and dried naturally at room temperature. The average weight (5 sample has been tested) was estimated to be 1.1 mg cm⁻² through a highly sensitive

balance with a precision down to 0.01 mg. Other samples also were fabricated at various times (4 min, 8 min, 12 min, 16 min) for the control experiment and realize the optimal deposition time.

Characterization

Field emission scanning electron microscope (FESEM, Quanta 450) and transmission electron microscope (TEM, JEOL JEM 2100F) with energy dispersive spectroscopy (EDS, Oxford) were employed to identify the morphology and structure. Also, the X-ray powder diffractometer (XRD, RigakuSmartLab) with monochromatic Cu K α (1.5418 Å) was further used to identify the phase and crystal structure.

in situ SEM Mechanical Characterization

The mechanical performance (i.e. Engineering Young's modulus, strength and compressive ability) was quantitatively analyzed inside SEM using picoindenter (HysitronTM PI85). Here, a diamond flat punch tip with 5 μm in diameter, with the load applied from the apex of the vertical axis, moving down with a displacement rate of 10 nm s⁻¹. Load-displacement curves were recorded accordingly. By using the nominal cross-sectional area and height of the structure, engineering stress and strain would be obtained.

Electrochemical test

The electrochemical performance of the sample was analyzed in a three-electrode system by using a platinum foil as the counter electrode, a saturated calomel electrode (SCE) as the reference electrode, and 2 M KOH as electrolyte.

For the positive electrode, the specific capacitance (F cm⁻²) can be calculated based on the following equation in galvanostatic charge/discharge (GCD) curves.³

$$C = \frac{2i \int V dt}{V^2 \left| \frac{V_f}{V_i} \right|} \quad (1)$$

And the capacity (mAh cm⁻²) was accordingly deduced from

$$Q = C \times V / 3.6$$

(2)

On the other hand, the specific capacitance of the negative electrode can be calculated

according to the following relation:

$$C = \frac{i\Delta t}{m\Delta V} \quad (3)$$

Where i (A) is the areal or mass current density, V_i (V) and V_f (V) is the initial and final voltage during discharging process, t or Δt (s) is the discharge time and V (V) is the potential range.

For the assembled two-electrode system, the charge balance was obtained according to following equation in cyclic voltammetry (CV) plots.⁴

$$\frac{m_+}{m_-} = \frac{(\int idV/v)_-}{(\int idV/v)_+} \quad (4)$$

Where m_+ (m_-) is the mass loading, v (mV s^{-1}) is the scan rate, V (V) is the voltage and $\int idV$ is the integral area of the cyclic voltammogram for the positive or negative electrode at 5 mV s^{-1} . According to the equation, the mass ratio of the positive electrode to positive electrode was found to be 1:3.75. The total electrode mass of the ASC was determined to be 5.22 mg cm^{-2} , based on the specific masses of the positive and negative electrodes, which were 1.1 mg cm^{-2} and 4.12 mg cm^{-2} respectively. However, the specific capacity should be calculated based on the total weight of the electrode including the weight of the gel electrolyte (PVA/KOH) within the pores of the electrode. In the final total weight of the assembled device (including the gel electrolyte), the weight was 6.73 mg cm^{-2} .

For the three-electrode measurement of the fiber supercapacitor, the areal was calculated according to $S = \pi \times d \times (\frac{d}{4} + l)$ (5)

Where the S is the surface area, d is diameter of the fiber (including the gel electrolyte) and l is the length of the active electrode materials.

The procedure for the assembly of the solid ASC is similar with our previous work.¹ Typically, 3 g of PVA was dissolved in 20 mL of distilled water with stirring at $90 \text{ }^\circ\text{C}$, when it became transparent followed by adding 10 mL of 0.3 g mL^{-1} KOH slowly. With further stirring for 2 h, the positive and negative electrodes were both immersed into the gel electrolyte for 5 min, respectively. Finally, they were assembled together after becoming solid in air temperature with following immersed into the gel

electrolyte again and protected with a heat shrinkable pipe.

The specific capacitance was obtained by using equation (1). The energy density (E , Wh kg⁻¹) and power density (P , W kg⁻¹) can be calculated by the following relations,

$$E = \frac{1}{2} \times CV^2 \quad (6)$$

$$P = \frac{E}{t} \quad (7)$$

Where C (F g⁻¹) is the specific capacitance, V (V) is voltage range of the ASC, and t (s) is corresponding discharge time.

The iR drop that was caused by the equivalent series resistance consisted of the electrode, electrolyte and contact resistance.⁵ And it can be measured by the vertical linear portion parallel to y -axis of the discharge profiles.

The procedures for assembly of SASC with strain sensor and nanogenerator can be found in Figure S25 and Figure S26, respectively. To integrate the SASC with flexible solar cell, the SASC was tightly fixed on the back side of the flexible solar cell (WARMSPACE, 1.5 V, 0.5 W, USA) using 3M tape.

As shown in Figure S1, the obvious peaks (111) and (200) belong to copper are observed after the electrodeposition process.⁶ The pattern corresponds to graphite (002) after the dip-coating process, indicating the multilayer and highly graphitic property of the GS.⁷ Although the real effect of multilayered graphene sheets maybe less than the expected of single layer graphene, it is still an promising candidate as electrode substrate.⁷⁸ And the peaks centered on (003) and other positions demonstrated the presence of the LDH structure⁶.

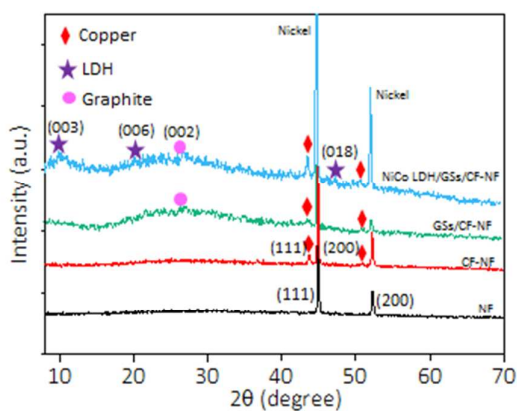


Figure S1. XRD patterns of the product fabricated with varying stage.

As shown in Figure S2, the electrodeposition time and current density were tuned to get the optimal morphology to deposit the GSs. Through the comparison of the sample deposited with from 10 to 90 s (Figure S2a-2d), too short time would lead to the thin deposited film while long time would cause the thick film and superior macro structure. Similar phenomenon was observed with the sample fabricated with various current density.

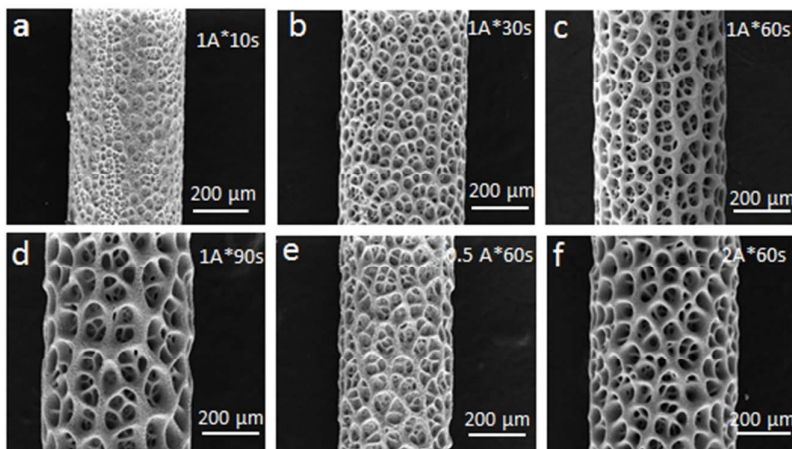


Figure S2. Optimizing the deposition time and current density to get the optimal feature of the CF-NF. (a) 1 A, 10 s. (b) 1 A, 30 s. (c) 1 A, 60 s. (d) 1 A, 90 s. (e) 0.5 A, 60 s. (f) 2 A, 60 s.

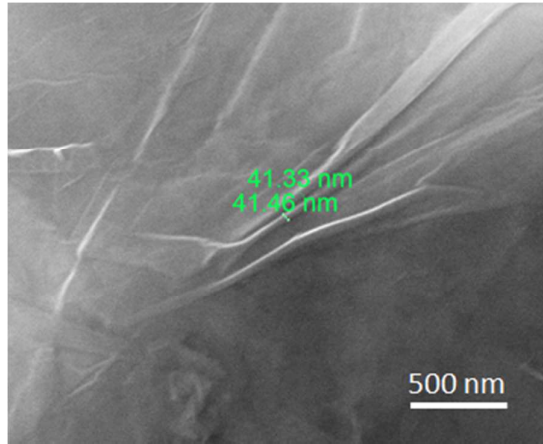


Figure S3. The thickness of graphene sheets which covered on the copper foam.

Mostly graphene was measured to be 1.53 nm thick and the Raman test indicates the high quality of the graphene sheets.

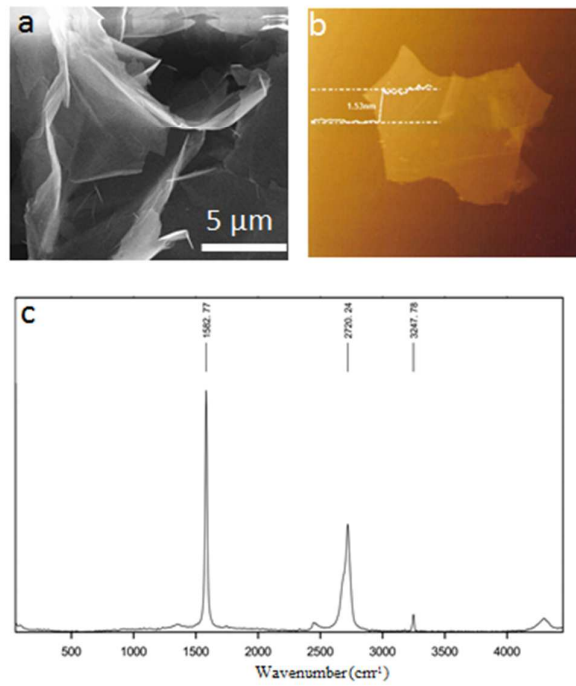


Figure S4. (a) SEM (b) AFM and (c) Raman characterization of the graphene.

As clearly observed in Figure S5, these elements (Co, Ni, O, C, and Cu) have homogeneous distribution among the whole nickel fiber. Additionally, the amount of nickel (2.5%) is slightly higher than that of the Co (2.5%), which derives from the nickel substrate. And the results confirm that no other impurity or element introduced into the sample.

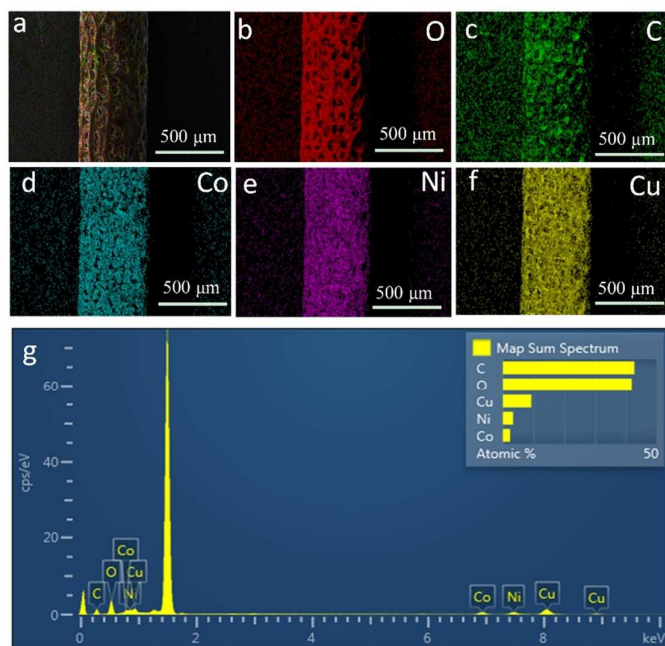


Figure S5. SEM-EDX characterization of NiCo LDH@GSs@CF-NF. (a) Overlap (b) O (c) C (d) Co (e) Ni (f) Cu element map of the NiCo LDH@GSs@CF-NF. (g) EDX element analysis results.

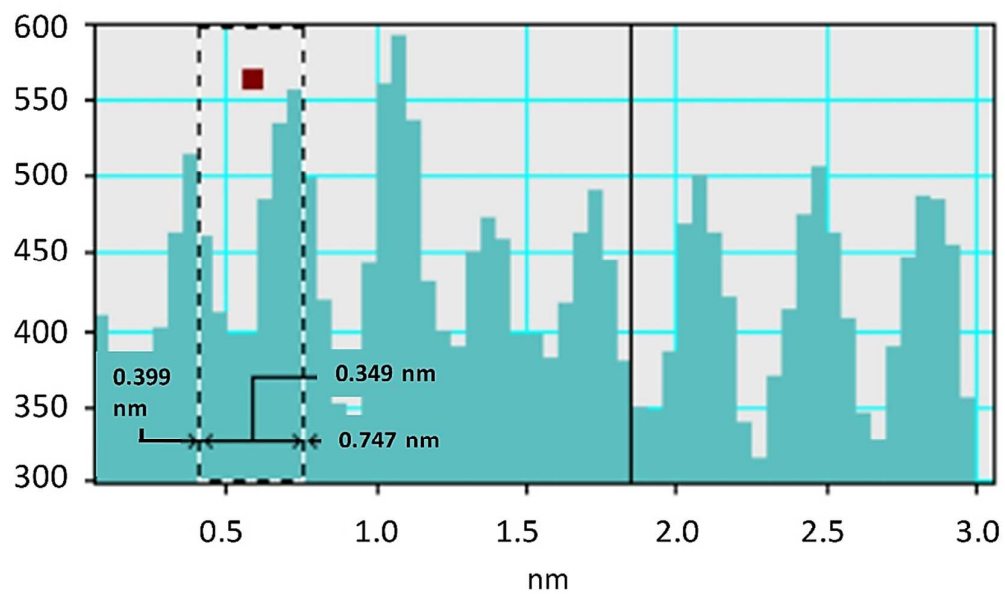


Figure S6. Spacing distance between graphene layer as marked in Figure 2j.

As shown below, the carbon accounts for 83.5 % that derived from the graphene sheets while the copper still existed (6.09%), suggesting the graphene has close adhesion on copper foam. Importantly, the same atomic ratio of the Ni (1.75%) and Co (1.69%) was observed, which further confirmed the equal content in the NiCo LDH.

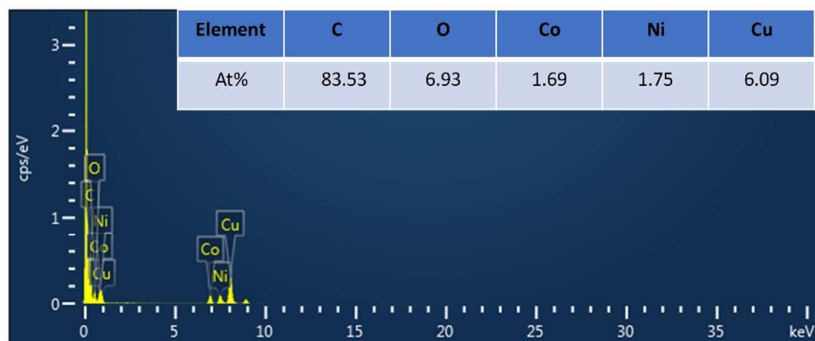


Figure S7. TEM-EDX results of the NiCo LDH@GSs.

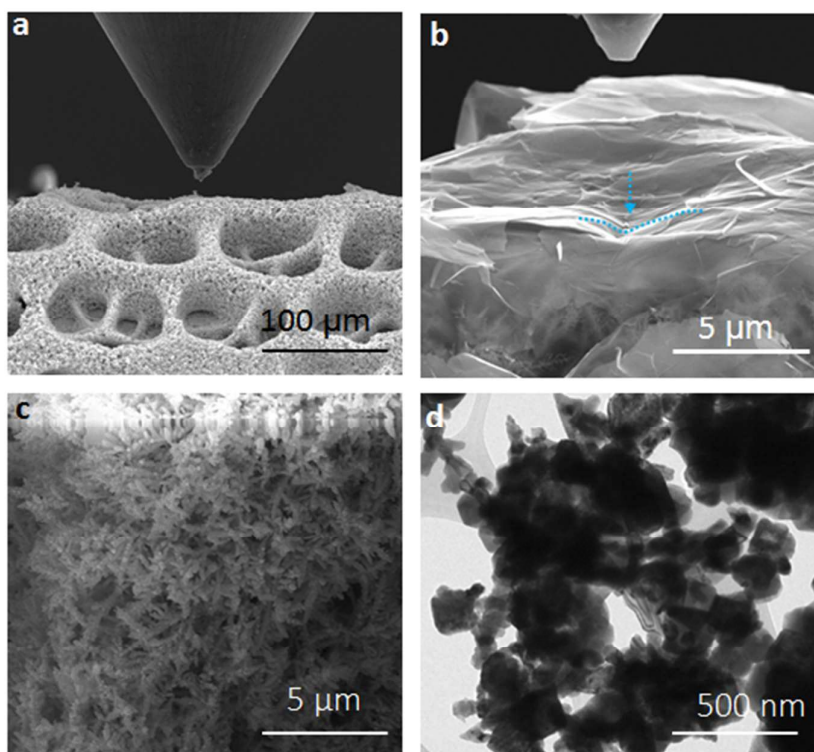


Figure S8. in situ nanoindentation test with a diamond indenter tip inside SEM. (a) Schematic illustration of the nanoindentation test. (b) Buckling of the graphene sheets. (c,d)SEM and TEM observation of the copper foam at micro scale.

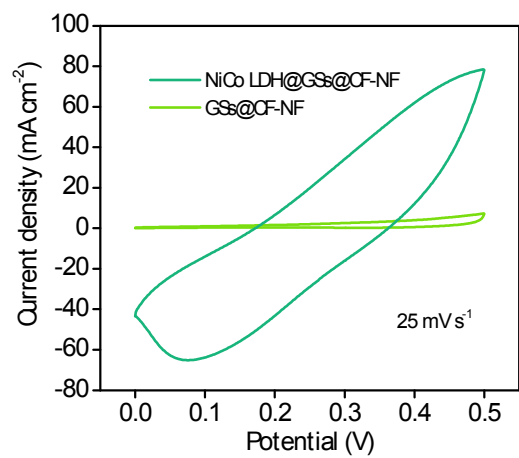


Figure S9. CV curves of NiCo LDH@GSs@CF-NF and GSs@CF-NF.

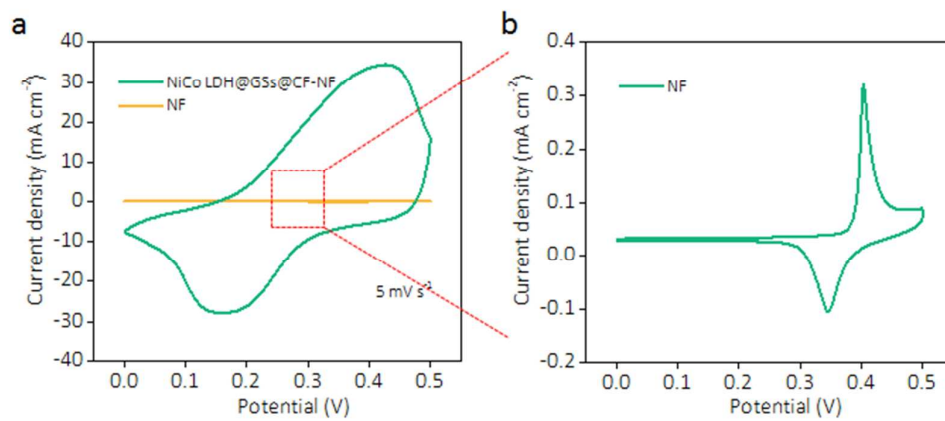


Figure S10. CV curves of (a) NiCo LDH@GSs@CF-NF and (b) NF.

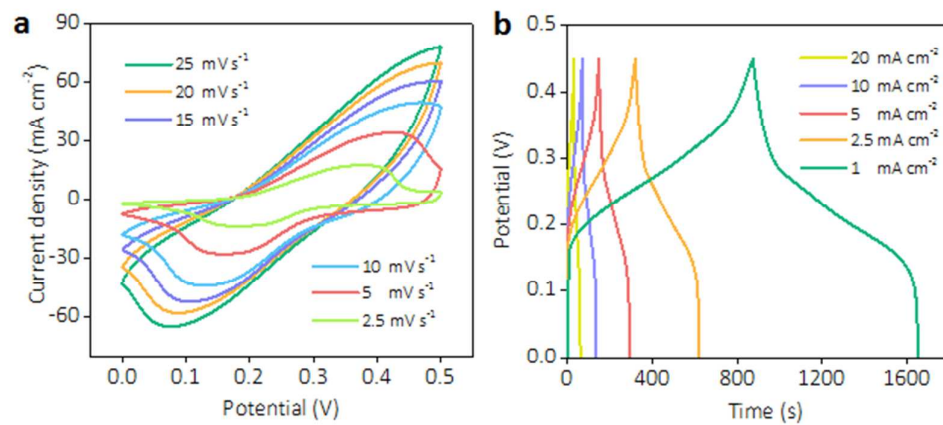


Figure S11. (a) CV and (b) GCD curves of NiCo LDH@GSSs@CF-NF.

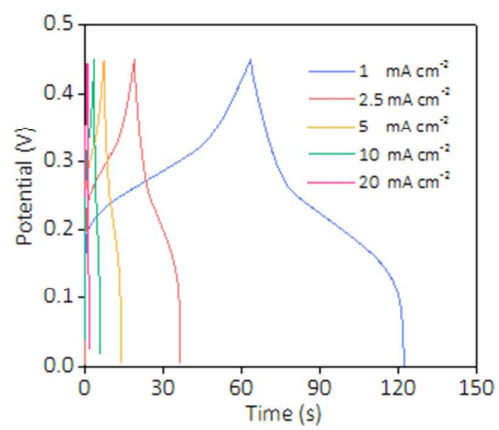


Figure S12. GCD curves of NiCo LDH@NF.

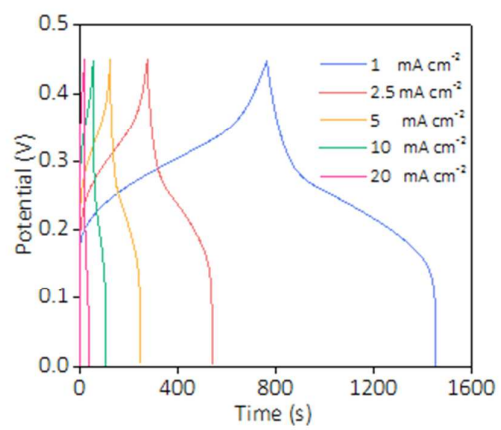


Figure S13. GCD curves of NiCo LDH@CF-NF.

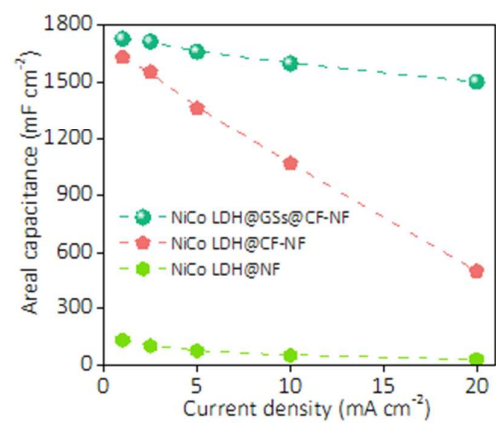


Figure S14. Areal capacitance as a function of current density.

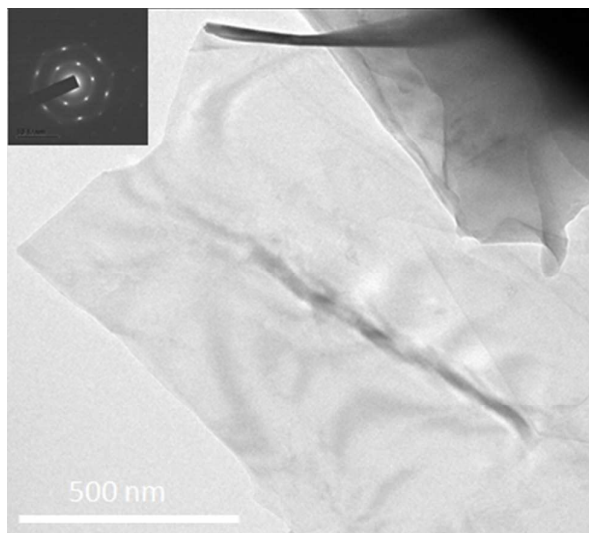


Figure S15. TEM and SAED pattern of the graphene sheet.

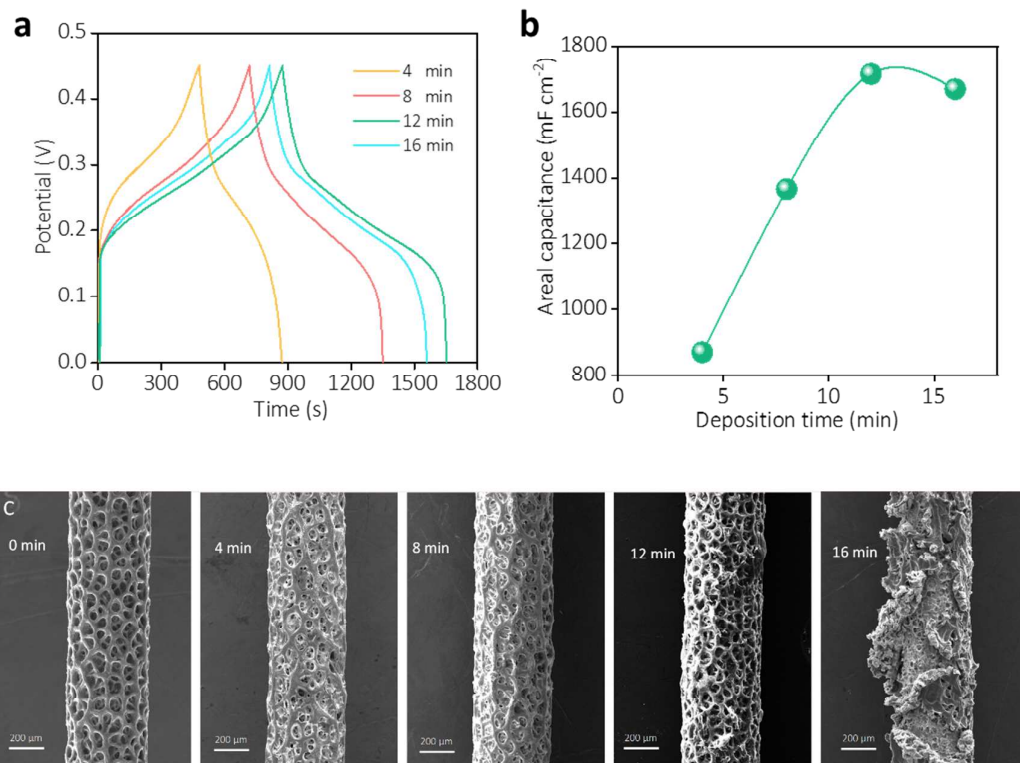


Figure S16. (a) GCD curves, (b) areal capacitance and (c) surface morphology of the NiCo LDH@GSs@CF-NF as a function of deposition time.

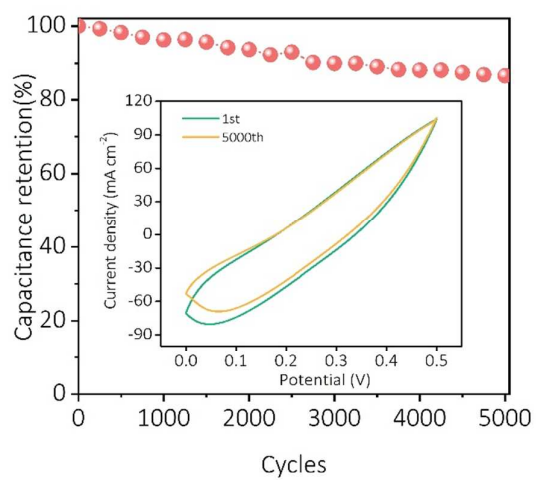


Figure S17. Cycling stability of NiCo LDH@GSs@CF-NF

To prepare the negative electrode, the activated carbon(AC) powder, acetylene black and poly-vinylidene fluoride (PVDF) were mixed together by a weight ratio of 8:1:1 in N-methylpyrrolidone (NMP) solution at 70 °C. The slurry then is painted on the nickel wire homogeneously. After drying at 80 °C to evaporate the NMP, the final sample can be obtained.

As show in Figure S18a, the AC show typical double-layer capacitive behavior at various scan rates, with further demonstrated by the GCD curves in Figure S18b. Accordingly, the sample show desired specific capacitance of 211.1 F g⁻¹ at 1 A g⁻¹ and superior rate capability of 88.1% when the current density increased to 10 A g⁻¹.

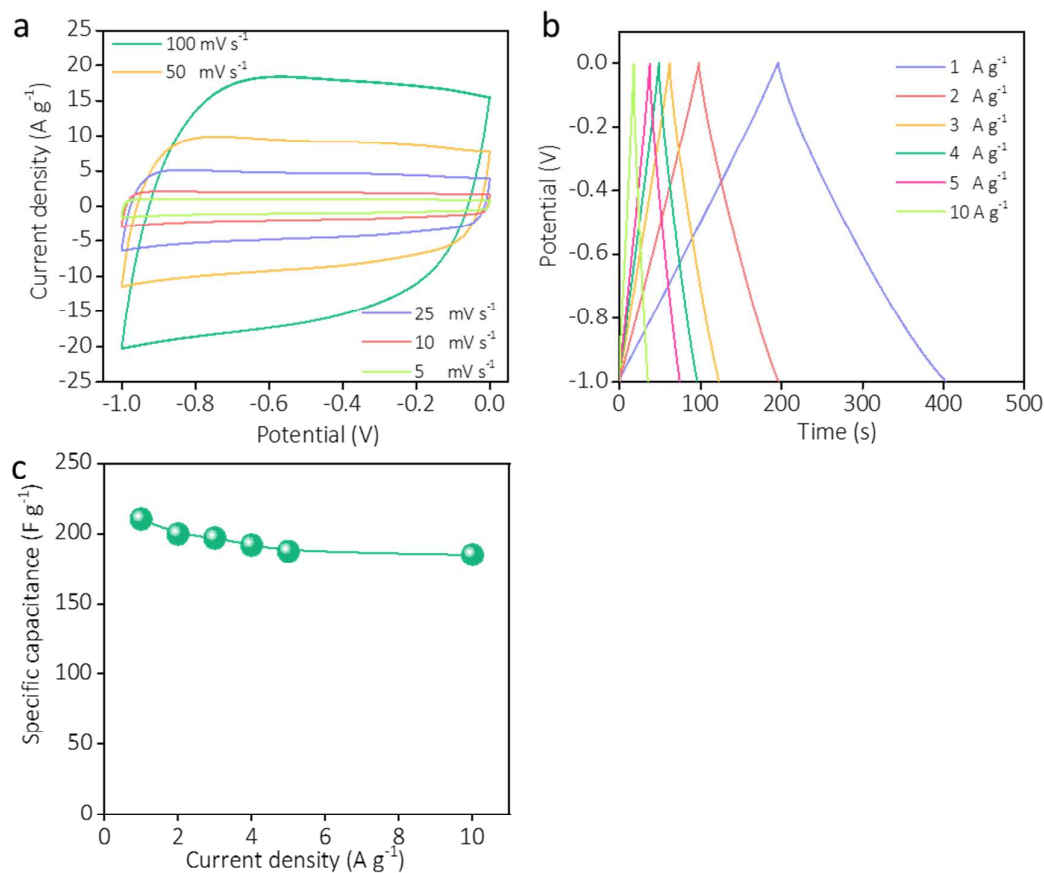


Figure S18. Electrochemical performance of the AC. (a) CV curves (b) GCD curves and (c) corresponding specific capacitance of the AC.

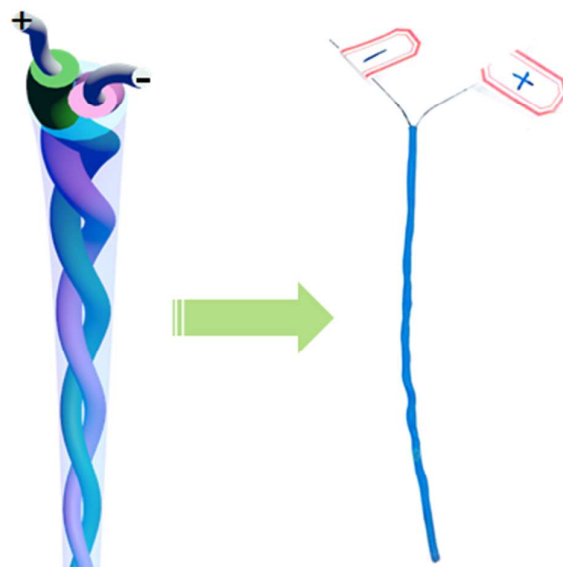


Figure S19. Schematic illustration and corresponding digital optical images of the assembled device.

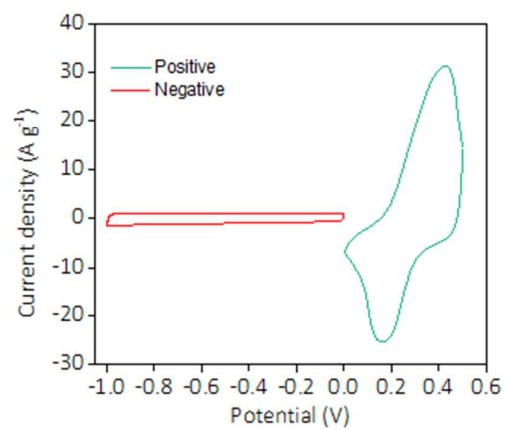


Figure S20. Working potential range of the positive and negative electrode

The device not only show high areal and specific capacitance as shown in Figure S19, but also show high length capacitance of 87.7 mF cm^{-1} at current density of 1 mA cm^{-2} , this value, to our knowledge, outperforming most device based on the similar materials, such as 79.8 mF cm^{-1} ,⁹ 42 mF cm^{-1} (0.5 A cm^{-3}),¹⁰ 31 mF cm^{-1} ,¹¹ 29.09 mF cm^{-1} (0.7 mA),¹² and 9.22 mF cm^{-1} .¹³

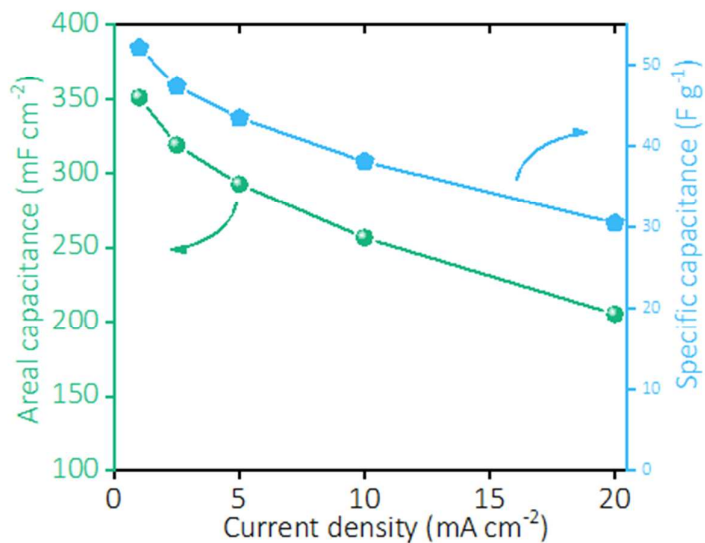


Figure S21. Areal and specific capacitance versus current density.

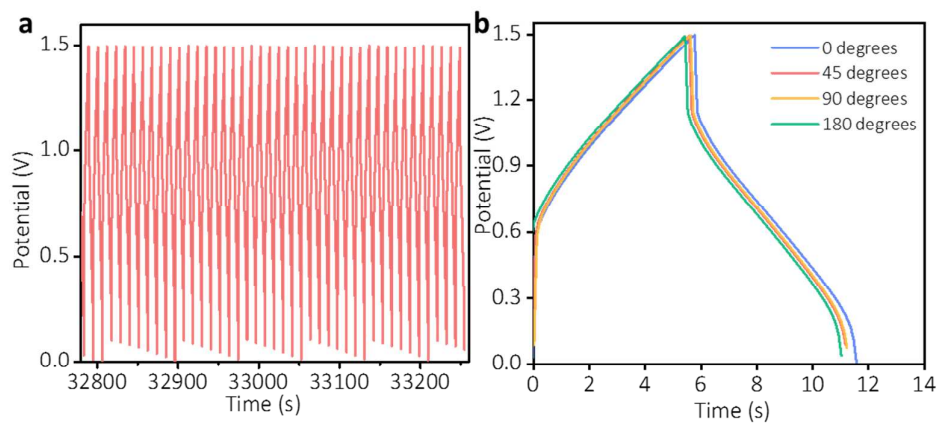


Figure S22. (a) Last GCD curves of the device for 3000 cycles and (b) Almost overlapped GCD curves of the device at 40 mA cm^{-2} .

The leakage current of the two connected fiber devices was measured in Figure S21a. After a rapid decrease from 812 μA to 230 μA within 500 s, it shows a stable current of 220 μA for an extended time. While the device still can remain $\sim 50\%$ voltage after 12000 s (Figure S23b), indicating the superior energy storage performance.

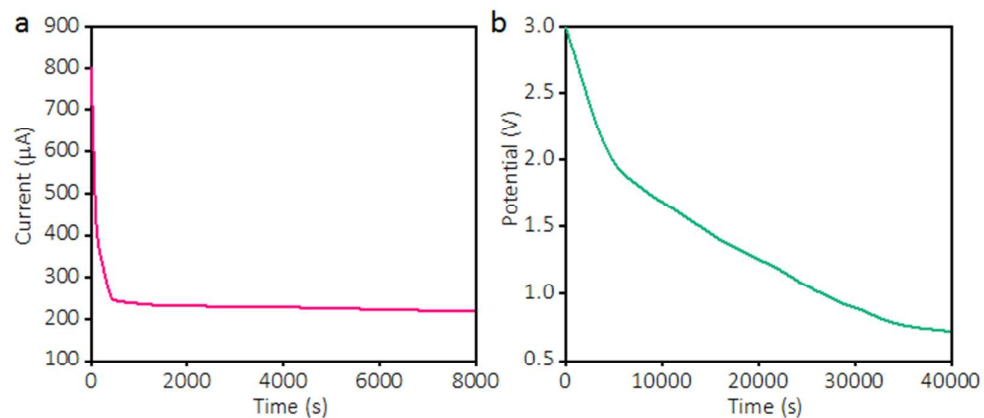


Figure S23. (a) Leakage current and (b) self-discharge curves of the two connected fiber devices.



Figure S24. The device can be easily fixed on the magnetic paper without using extra force.

The strain sensor was fabricated according to other reports elsewhere.¹⁴ Briefly, the pristine flexible polyester yarn was coated with a thin nickel layer firstly according to our previous paper.¹ Then the Ni-coated yarn was immersed into 5 mg mL⁻¹ of graphene oxide (GO) solution (Heng Qiu Tech Co., Ltd, Jiang Su) with hydrothermal reaction at 80 °C for 6 h. After further reduction in 0.1 M ascorbic at 90 °C for 2 h and washed with DI water, the final strain sensor was obtained when subsequent dried in oven. Then the as-synthesized strain sensor was rationally assembled with the SASC as shown in Figure 6a. Variation of the corresponding resistance with strain was conducted by generating an amperometric *i*-*t* curve in working station.

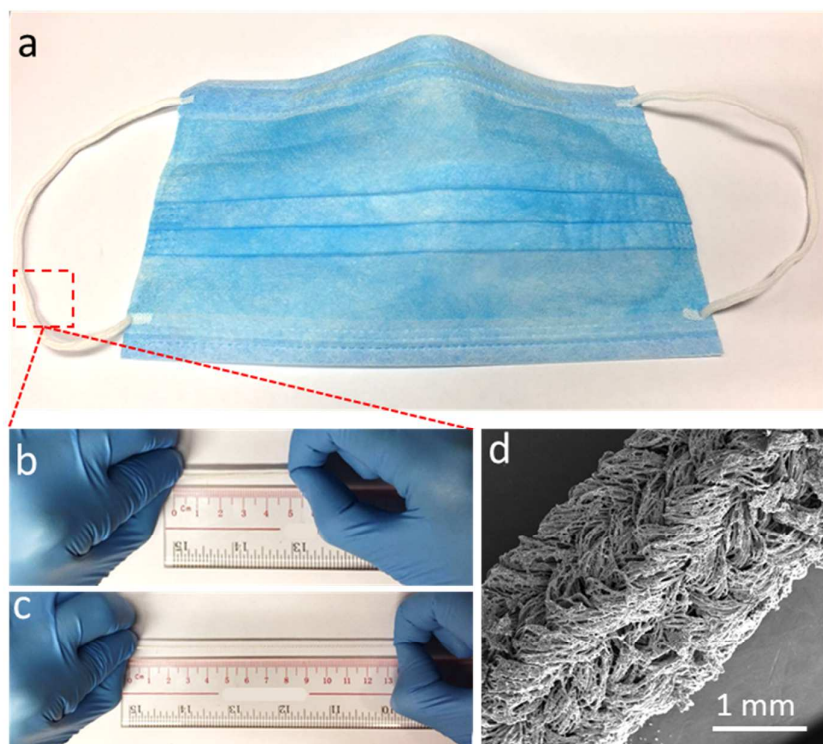


Figure S25. (a) Optical images of wasted disposable lab masks. (b-c) Excellent flexibility of the polyester yarn and (d) SEM images of the graphene coated on the nickel-coated yarn.

The procedure for fabrication of the nanogenerator was shown in our previous article.¹⁵ And the schematic illustration for assembling the fiber supercapacitor with nanogenerator can be found in main article. Below is corresponding optical digital images. Note that the pressure force and frequency applied on the nanogenerator is 1000 N and 3 Hz, respectively.

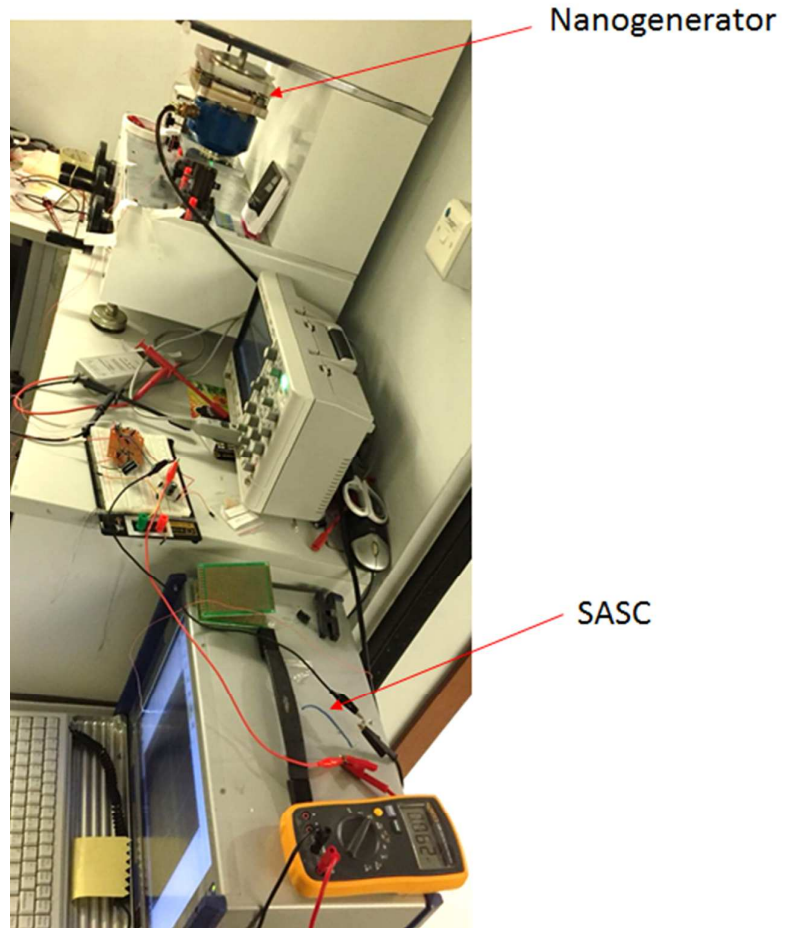


Figure S26. Using the nanogenerator to charge the SASC.

Table S1. The comparison of the electrochemical behavior of our work with other reported fiber supercapacitor device.

Electrode Material	Electrolyte	C_a , single (mF cm ⁻²)	Rate capability	C_s ,device (mF cm ⁻²)	E_a , device (μwh cm ⁻²)	P_a , device (μw cm ⁻²)	Reference
CuO@FeCo	PVA/KOH	866	82.1%		93.75		6
LDH//AC			2.5 to 20 mA cm ⁻²				
TiN@C// TiN@C	PVA/KOH	11.15		19.4	2.69	809	13
NiO/Ni(OH) ₂	PVA/KOH	404.1	82.2%	31.6	11	330	16
/PEDOT//AC			4 to 24 mA cm ⁻²				
Ni(OH) ₂ //OMC	PVA/KOH	195	36%	35.67	10		17
			0.5 to 2.5 mA				
NiCo ₂ O ₄ //NiCo ₂ O ₄	PVA/KOH	750	91%				18
			5 to 80 mV s ⁻¹				
PPy@MnO ₂ @rGO	PVA/	486		103	9.2	1330	11
//PPy@MnO ₂ @rGO	H ₃ PO ₄						
O							
Pen ink/Ni//	PVA/	9.5			2.7	42	19
Pen ink/Ni	H ₂ SO ₄						
MnO ₂ /PEDOT/CN	PVA/Na ₂ SO ₄	715	68.8%	213.5	96	270	20
T//VN/CNT			1 to 10 mA cm ⁻²				
NiCoS//rGO	PVA/LiOH			127	48.7	553	21
MnO ₂ /CNT/graphene/Nickel tube	PVA/LiCl			31	3.1	120	22
MXene(Ti ₃ C ₂ Tx)//							
MXene(Ti ₃ C ₂ Tx)	PVA/H ₂ SO ₄			328	7.3	132	23
MOF-templated							
CNTFs@ZnCo ₂ O ₄							
@Zn-Co-S HA//		1347.77		117.18	32.1	698.42	24
CNTFs@H-Co ₃ O ₄	PVA/KOH						
@CoNC HA							
NiCo	PVA/KOH	1729.4	86.9% from 1 to	350.9	109.6	749.5	Our work
LDH@GSs@CF-			20 mA cm⁻²				
NF//AC							

Movie S1. The curved individual SASC was twined around a finger to power a digital watch;

Movie S2. A motor fan was driven by the connected SASC.

Movie S3. A pocket calculator was powered by the SASCs.

Movie S4. The strain sensor was assembled with the SASC.

Reference

- (1) Gao, L.; Surjadi, J. U.; Cao, K.; Zhang, H.; Li, P.; Xu, S.; Jiang, C.; Song, J.; Sun, D.; Lu, Y. Flexible Fiber-Shaped Supercapacitor Based on Nickel–Cobalt Double Hydroxide and Pen Ink Electrodes on Metallized Carbon Fiber. *ACS Appl. Mater. Interfaces* **2017**, *9*, 5409–5418.
- (2) Gao, L.; Cao, K.; Zhang, H.; Li, P.; Song, J.; Surjadi, J. U.; Li, Y.; Sun, D.; Lu, Y. Rationally Designed Nickel Oxide Ravines@iron Cobalt-Hydroxides with Largely Enhanced Capacitive Performance for Asymmetric Supercapacitors. *J. Mater. Chem. A* **2017**, *5*, 16944–16952.
- (3) Mai, L.; Minhas-Khan, A.; Tian, X.; Hercule, K. M.; Zhao, Y.; Lin, X.; Xu, X. Synergistic Interaction between Redox-Active Electrolyte and Binder-Free Functionalized Carbon for Ultrahigh Supercapacitor Performance. *Nat. Commun.* **2013**, *4*, 2923.
- (4) Zhao, B.; Chen, D.; Xiong, X.; Song, B.; Hu, R.; Zhang, Q.; Rainwater, B. H.; Waller, G. H.; Zhen, D.; Ding, Y.; Chen, Y.; Qu, C.; Dang, D.; Wong, C.-P.; Liu, M. A High-Energy, Long Cycle-Life Hybrid Supercapacitor Based on Graphene Composite Electrodes. *Energy Storage Mater.* **2017**, *7*, 32–39.
- (5) An, K. H.; Kim, W. S.; Park, Y. S.; Moon, J. M.; Bae, D. J.; Lim, S. C.; Lee, Y. S.; Lee, Y. H. Electrochemical Properties of High-Power Supercapacitors Using Single-Walled Carbon Nanotube Electrodes. *Adv. Funtional Mater.* **2001**, *11*, 387–392.
- (6) Li, Z.; Shao, M.; Zhou, L.; Zhang, R.; Zhang, C.; Han, J.; Wei, M.; Evans, D. G.; Duan, X. A Flexible All-Solid-State Micro-Supercapacitor Based on Hierarchical CuO@layered Double Hydroxide Core-Shell Nanoarrays. *Nano Energy* **2016**, *20*, 294–304.
- (7) Xiong, G.; He, P.; Wang, D.; Zhang, Q.; Chen, T.; Fisher, T. S. Hierarchical Ni-Co Hydroxide Petals on Mechanically Robust Graphene Petal Foam for High-Energy Asymmetric Supercapacitors. *Adv. Funct. Mater.* **2016**, *26*, 5460–5470.
- (8) Song, Y.; Cai, X.; Xu, X.; Liu, X.-X. Integration of Nickel–cobalt Double

Hydroxide Nanosheets and Polypyrrole Films with Functionalized Partially Exfoliated Graphite for Asymmetric Supercapacitors with Improved Rate Capability. *J. Mater. Chem. A* **2015**, *3*, 14712–14720.

- (9) Li, P.; Li, J.; Zhao, Z.; Fang, Z.; Yang, M.; Yuan, Z.; Zhang, Y.; Zhang, Q.; Hong, W.; Chen, X.; Yu, D. A General Electrode Design Strategy for Flexible Fiber Micro-Pseudocapacitors Combining Ultrahigh Energy and Power Delivery. *Adv. Sci.* **2017**, *4*, 1700003.
- (10) Pan, Z.; Zhong, J.; Zhang, Q.; Yang, J.; Qiu, Y.; Ding, X.; Nie, K.; Yuan, H.; Feng, K.; Wang, X.; Xu, G.; Li, W.; Yao, Y.; Li, Q.; Liu, M.; Zhang, Y. Ultrafast All-Solid-State Coaxial Asymmetric Fiber Supercapacitors with a High Volumetric Energy Density. *Adv. Energy Mater.* **2018**, *8*, 1702946.
- (11) Huang, Y.; Hu, H.; Huang, Y.; Zhu, M.; Meng, W.; Liu, C.; Pei, Z.; Hao, C.; Wang, Z.; Zhi, C. From Industrially Weavable and Knittable Highly Conductive Yarns to Large Wearable Energy Storage Textiles. *ACS Nano* **2015**, *9*, 4766–4775.
- (12) Nagaraju, G.; Sekhar, S. C.; Yu, J. S. Utilizing Waste Cable Wires for High-Performance Fiber-Based Hybrid Supercapacitors: An Effective Approach to Electronic-Waste Management. *Adv. Energy Mater.* **2018**, *8*, 1702201.
- (13) Sun, P.; Lin, R.; Wang, Z.; Qiu, M.; Chai, Z.; Zhang, B.; Meng, H.; Tan, S.; Zhao, C.; Mai, W. Rational Design of Carbon Shell Endows TiN@C Nanotube Based Fiber Supercapacitors with Significantly Enhanced Mechanical Stability and Electrochemical Performance. *Nano Energy* **2017**, *31*, 432–440.
- (14) Pu, X.; Li, L.; Liu, M.; Jiang, C.; Du, C.; Zhao, Z.; Hu, W.; Wang, Z. L. Wearable Self-Charging Power Textile Based on Flexible Yarn Supercapacitors and Fabric Nanogenerators. *Adv. Mater.* **2016**, *28*, 98–105.
- (15) Chen, S.; Tao, X.; Zeng, W.; Yang, B.; Shang, S. Quantifying Energy Harvested from Contact-Mode Hybrid Nanogenerators with Cascaded Piezoelectric and Triboelectric Units. *Adv. Energy Mater.* **2017**, *7*, 1601569.

- (16) Yang, H.; Xu, H.; Li, M.; Zhang, L.; Huang, Y.; Hu, X. Assembly of NiO/Ni(OH)₂/PEDOT Nanocomposites on Contra Wires for Fiber-Shaped Flexible Asymmetric Supercapacitors. *ACS Appl. Mater. Interfaces* **2016**, *8*, 1774–1779.
- (17) Dong, X.; Guo, Z.; Song, Y.; Hou, M.; Wang, J.; Wang, Y.; Xia, Y. Flexible and Wire-Shaped Micro-Supercapacitor Based on Ni(OH)₂-Nanowire and Ordered Mesoporous Carbon Electrodes. *Adv. Funct. Mater.* **2014**, *24*, 3405–3412.
- (18) Ramadoss, A.; Kang, K.-N.; Ahn, H.-J.; Kim, S.-I.; Ryu, S.-T.; Jang, J.-H. Realization of High Performance Flexible Wire Supercapacitors Based on 3-Dimensional NiCo₂O₄/Ni Fibers. *J. Mater. Chem. A* **2016**, *4*, 4718–4727.
- (19) Fu, Y.; Cai, X.; Wu, H.; Lv, Z.; Hou, S.; Peng, M.; Yu, X.; Zou, D. Fiber Supercapacitors Utilizing Pen Ink for Flexible/Wearable Energy Storage. *Adv. Mater.* **2012**, *24*, 5713–5718.
- (20) Zhang, Q.; Wang, X.; Pan, Z.; Sun, J.; Zhao, J.; Zhang, J.; Zhang, C.; Tang, L.; Luo, J.; Song, B.; Zhang, Z.; Lu, W.; Li, Q.; Zhang, Y.; Yao, Y. Wrapping Aligned Carbon Nanotube Composite Sheets around Vanadium Nitride Nanowire Arrays for Asymmetric Coaxial Fiber-Shaped Supercapacitors with Ultrahigh Energy Density. *Nano Lett.* **2017**, *17*, 2719–2726.
- (21) Chen, Y.; Xu, B.; Wen, J.; Gong, J.; Hua, T.; Kan, C.-W.; Deng, J. Design of Novel Wearable, Stretchable, and Waterproof Cable-Type Supercapacitors Based on High-Performance Nickel Cobalt Sulfide-Coated Etching-Annealed Yarn Electrodes. *Small* **2018**, *14*, 1704373.
- (22) Kang, Q.; Zhao, J.; Li, X.; Zhu, G.; Feng, X.; Ma, Y.; Huang, W. A Single Wire as All-Inclusive Fully Functional Supercapacitor. *Nano Energy* **2017**, *32*, 201–208.
- (23) Hu, M.; Li, Z.; Li, G.; Hu, T.; Zhang, C.; Wang, X. All-Solid-State Flexible Fiber-Based MXene Supercapacitors. *Adv. Mater. Technol.* **2017**, *2*, 1–6.
- (24) Zhao, J.; Li, H.; Li, C.; Zhang, Q.; Sun, J.; Wang, X.; Guo, J.; Xie, L.; Xie, J.;

He, B.; Zhou, Z.; Lu, C.; Lu, W.; Zhu, G.; Yao, Y. MOF for Template-Directed Growth of Well-Oriented Nanowire Hybrid Arrays on Carbon Nanotube Fibers for Wearable Electronics Integrated with Triboelectric Nanogenerators. *Nano Energy* **2018**, *45*, 420–431.